LAWRENCE
LIVERMORE
NATIONAL
LABORATORY

UCRL-JRNL-208963

Synthesis of TiO2 Nanoparticles on the Au(111) Surface

J. Biener, E. Farfan-Arribas, M. M. Biener, C. M. Friend, R. J. Madix

January 12, 2005

Surface Science

To be submitted

Jan. 11, 2005

Synthesis of TiO_2 Nanoparticles on the Au(111) Surface

Jürgen Biener[a,c], Enrique Farfan-Arribas[b], Monika Biener[a], Cynthia M. Friend[a,*] and Robert J. Madix[b]

[a]Department of Chemistry and Division of Engineering and Applied Sciences
Harvard University, 12 Oxford Street, Cambridge, Massachusetts 02138
[b]Chemical Engineering Department, Stanford University
Stanford, California 94305-5025
[c]Lawrence Livermore National Laboratory
7000 East Ave, Livermore, CA 94550 USA

Abstract

The growth of titanium oxide nanoparticles on reconstructed Au(111) surfaces was investigated by scanning tunneling microscopy and X-ray photoelectron spectroscopy. Ti was deposited by physical vapor deposition at 300 K. Regular arrays of titanium nanoparticles form by preferential nucleation of Ti at the elbow sites of the herringbone reconstruction. Titanium oxide clusters were synthesized by subsequent exposure to O_2 at 300 K. Two- and three-dimensional titanium oxide nanocrystallites form during annealing in the temperature range from 600 to 900 K. At the same time, the Au(111) surface assumes a serrated, <110> oriented step-edge morphology, suggesting step-edge pinning by titanium oxide nanoparticles. The oxidation state of these titanium oxide nanoparticles varies with annealing temperature. Specifically, annealing to 900 K results in the formation of stoichiometric TiO_2 nanocrystals as judged by the observed XPS binding energies. Nano-dispersed TiO_2 on Au(111) is an ideal system to test the various models explaining the enhanced catalytic reactivity of supported Au nanoparticles.

[*] **Corresponding Author. Email: cfriend@deas.harvard.edu**

Introduction

Metal oxides are of considerable interest because of their technological importance, e.g. in the field of heterogeneous catalysis, where they are used as catalyst supports for a wide variety of metals. The interaction of the adsorbed metal particles with the oxide support is complex and gives rise to interesting phenomena such as the strong metal support interaction (SMSI). This term describes the change in catalytic activity (favoring hydrogenation) observed when group VIII B metals supported on reducible oxides (TiO_2, TaO_5, CeO_2, NbO) are annealed in a reducing atmosphere [1]. Transition metal oxides are also used to support other oxides in the so-called monolayer catalysts. For example, V_2O_5/TiO_2 systems are used for the partial oxidation of methanol, and have been extensively studied in single crystal as well as in powder form [2-5].

More recently, the interaction of metal oxides, especially TiO_2 [6-10], with small Au particles has been the subject of intense study. Small gold particles supported on metal oxides, including TiO_2, are highly reactive oxidation catalysts, and a pronounced particle size effect was observed. This work has generated considerable controversy as to the underlying reason for the high activity of supported Au nanoparticles. Various models have been proposed to explain the unusual catalytic properties of gold nanoclusters ranging from metal-support interactions to finite size effects [11]. More recently, undercoordinated Au atoms have been linked to the enhanced reactivity of supported Au nanoparticles [12-14].Yet another explanation involves oxygen spillover from the oxide to the Au nanoparticles thus providing a source of oxygen.

In this study, we developed a method to synthesize TiO_2 nanoparticles on Au to contribute to a better understanding of Au-based catalysts with an emphasis on the fundamental interactions between TiO_2 and gold. This work builds on our earlier studies of the growth of MoO_3 on Au(111) [15-18]. Herein, we demonstrate that we are able to generalize the growth of metal oxide nanostructures on the reconstructed Au(111)-"herringbone" surface to TiO_2, which is a three-dimensional metal oxide. Previous studies of Ni [19], Fe [20], Co [21], and Mo [18, 22, 23] on Au(111) show that metal particles nucleate at the elbow sites of the herringbone reconstruction of the gold surface when deposited via physical vapor deposition (PVD). In the case of Mo, metallic nanoparticles have been converted to two-dimensional nanocrystalline MoS_2 [22] and MoO_3 particles [16], respectively. The objective of the work presented here was to systematically synthesize and characterize titanium oxide nanoparticles on reconstructed Au(111) surfaces which may then be used as models for reactivity studies of isolated oxide nanoparticles.

Experimental

Scanning tunneling microscope (STM) studies were performed in a commercial ultrahigh vacuum (UHV) system (Omicron) with a base pressure of ~$5x10^{-11}$ mbar. The system has separate compartments for sample preparation and sample characterization. The characterization compartment is equipped with instrumentation for scanning probe microscopy (SPM), Auger electron spectroscopy (AES) and low energy electron diffraction (LEED). The X-ray photoemission spectroscopy (XPS) experiments were performed in a separate UHV system with base pressure of ~3 x 10^{-10} mbar [24]. The analysis chamber of this system is equipped with a LEED optics, a Perkin-Elmer 04-548 dual-anode X-ray source, a SPECS EA-10 Plus

hemispherical energy analyzer, a UTI 100c quadrupole mass spectrometer (QMS), and a gas needle doser.

The Au(111) sample was cleaned by cycles of Ar^+ sputtering at room temperature (15-60 min / 500-1000 eV / 4 μA) followed by annealing in vacuum (10 min at 900 K followed by 20-60 min at 700 K). This procedure was repeated until no contaminants were detected by means of AES or XPS. In the SPM system, the Au(111) single crystal was heated by a PBN heating element, and the temperature was monitored using an optical pyrometer calibrated against a thermocouple (Type K). In the XPS system, the Au(111) sample was attached to tantalum foil which was resistively heated via the two tungsten wires allowing sample temperatures up to 950 K. In this setup, the temperature was measured by a thermocouple (Type K) inserted into a hole on the side of the Au(111) crystal.

In the STM system, titanium (Aldrich, 99.99%) was evaporated from rod material (2.0 mm diam.) using an electron beam evaporator (800 V / ~ 30 mA). The deposition rate (~0.1 ML Ti min$^-$1) was monitored continuously by a flux monitor measuring the ion flux, which is proportional to the flux of evaporated atoms. Initially the deposition rate was calibrated using a quartz thickness monitor. A home-built metal evaporator was used in the XPS system. Here, the Ti source was a resistively heated (1.25 A) titanium filament (0.008" in diameter, 99.9999% pure, ESPI Products). The amount of deposited titanium was determined by XPS. The filament is surrounded by a water-cooled shield so as to maintain the pressure below 3 x 10^{-9} mbar during evaporation.

Titanium oxide nanoparticles were synthesized by oxidizing evaporated titanium using molecular oxygen (Matheson, research purity grade). The purity of all gases was periodically checked with a residual gas analyzer. STM images were collected at room temperature, and Z-channel and I-channel images were obtained simultaneously. Etched $Pt_{0.8}$ $Ir_{0.2}$ tips from Molecular Imaging were used for imaging. The bias voltage was set between -1.5 V and + 2.0 V.

Results and Discussion

Well-ordered arrays of Ti nanoclusters were prepared on the reconstructed Au(111) surface by PVD of Ti at 300 K, as alloying and bulk diffusion were observed at higher deposition temperatures [25]. An example is shown in Figure 1a for a Ti coverage of 0.1 ML. The elbow sites of the herringbone reconstruction serve as selective nucleation sites for the growth of titanium islands. The preferential nucleation of metals at the elbow sites of the herringbone reconstruction is a common phenomenon and was previously reported for Ni, Co, Mo and Fe [18-23]. The results regarding Ti deposition on Au(111) will be published in more detail elsewhere [25]. Briefly, exclusively monolayer islands with an apparent height of ~0.2 nm are observed in the coverage range from 0.05 to 0.25 ML, and both size and density of the Ti islands increase with increasing Ti coverage. Second layer features appear reaching a Ti coverage of ~0.5 ML, and distinct particles are evident up to a Ti coverage of 1 ML. The observation of a depletion zone around the Au step edges (Fig. 1a) suggests local alloying, even at deposition temperatures as low as 300 K.

Titanium oxide nanoparticles were synthesized by subsequent oxidation via O_2 exposure ($5x10^{-5}$ mbar for 200 s) at 300 K (Fig. 1b). The oxidation of titanium leads to (i) a more disordered arrangement of the clusters, (ii) an increase in height (from ~0.2 nm to ~0.28 – 0.38 nm), and (iii) and increase in diameter (from ~3 nm to 1.8 – 8.5 nm). The formation of titanium oxide was confirmed by Auger electron spectroscopy (data not shown). Furthermore, additional protrusions appear at step edges (Fig. 1b), which suggests oxygen-driven de-alloying of previously alloyed titanium. The oxidation-induced rearrangement of the protrusions at room temperature suggests a relatively high mobility of titanium oxide on Au(111), consistent with the streaky appearance of the STM images.

Subsequent annealing leads to morphological changes in both the titanium oxide and the Au(111) surface. After annealing at 600 K (Fig. 1c), the density of the titanium oxide clusters decreases sharply, and the particles assume a somewhat more regular shape. Both height and diameter of the titanium oxide particles further increase upon annealing to 600 K to ~ 0.5 nm and ~5 nm, respectively. Simultaneously, the ordered herringbone pattern of clean Au(111) reappears (Fig. 1c inset).

Faceted three-dimensional titanium oxide crystallites with an apparent height of ~0.6 - 1.2 nm and a diameter of several nm decorate both step-edges and terraces after further annealing at 900 K (Fig. 1d). The step edges of the Au surface assume a serrated, <110> oriented morphology. This seems to be caused by step-edge pinning by titanium oxide crystallites in combination with a high step-edge mobility of Au(111) at 900 K. The herringbone pattern of the Au(111) surface is disturbed in the vicinity of the titanium oxide particles (Fig 1d, inset). AE spectra collected from this surface reveal an O_{512} :Ti_{387} AES peak ratio of ~ 1.5, consistent with a Ti oxidation state of +4 [26].

The morphology of titanium oxide nanoparticles also depends on the initial titanium coverage (Fig. 2). Using a Au(111) surface originally covered with ~0.25 ML metallic titanium as a starting point, both 2- and 3-dimensional titanium oxide particles with either a triangular or a hexagonal crystal shape are observed with STM (Fig. 2a). Approximately 13 % of the Au(111) surface is covered by 2-dimensional titanium oxide islands and ~ 7 % by 3-dimensional titanium oxide crystallites. Both 2D and 3D titanium oxide particles exhibit a typical feature size of ~5 nm. The apparent height of the 2D features changes with the tunneling conditions: applying bias voltages of -1.5 V and +2.5 V, respectively, results in apparent heights of 0.15 nm and 0.3 nm. The 3-dimensional titanium oxide crystallites exhibit an apparent height of ~0.6-0.8 nm. Both 2-dimensional and 3-dimensional titanium oxide crystallites are aligned along the close-packed <110> directions of the underlying Au(111). Based on previous studies of MoO_3 nanostructures, we postulate that this preferential alignment is due to differential diffusion kinetics, and not a thermodynamic preference for this alignment.

Additional features such as needle-like titanium oxide crystallites are observed for higher Ti starting coverages. Figure 2b shows a STM image obtained after oxidation of 0.5 ML titanium and subsequent annealing at 900 K. The coverage of two- and three-dimensional titanium oxide particles further increases to ~15% and ~20%, respectively. Needle-like three-dimensional features (Fig 3b, inset I) decorate step-edges, and embedded hexagonal-shaped titanium oxide crystals (Fig 3b, inset II) appear close to step edges. Two-dimensional features now exhibit an

apparent height of ~0.3 nm, and a diameter of ~10 - 20 nm. The predominately triangular-shaped three-dimensional titanium oxide crystallites (Fig 3b, inset III) are much higher, exhibiting an apparent height of ~1 - 2.5 nm, and a diameter of ~6 - 12 nm.

During annealing at 900 K, the titanium oxide islands develop a crystalline structure as revealed by STM. Specifically, the high resolution STM of a two-dimensional titanium oxide island shown in figure 3 reveals two sets of rows separated by 1.44 nm and rotated about 120° against each other. These rows are rotated ~ 10° against the close-packed <110> directions of the underlying Au(111) crystal which determine the shape of the crystallite (Fig. 3a). Additional second layer features on top of the titanium oxide crystal seem to exhibit a $(\sqrt{3} \times \sqrt{3})R30°$ relationship towards the underlying structure of the titanium oxide crystal (Fig. 3b). Although these observations clearly demonstrate the well-ordered nature of the synthesized titanium oxide, a LEED structure was not observed.

The O_{512} / Ti_{387} AES peak ratios obtained from titanium oxide nanoparticles after annealing at 900 K fluctuates between 1.1 and 1.6, indicating that in some cases titanium was not completely oxidized. In an attempt to prepare fully oxidized titanium oxide nanoparticles on Au(111), a surface covered with 0.25 ML titanium oxide particles prepared by the procedure described above was further annealed in oxygen at 600 K (5×10^{-5} mbar, 15 min). STM reveals that the morphology of the titanium oxide particles is very similar before and after the second oxidation step (data not shown). However, the surface becomes much more difficult to image, suggesting further oxidation of titanium. Indeed, AE spectra reveal an increase in the oxygen coverage of ~30% (the O_{512} / Ti_{387} AES peak increases from ~1.35 to ~ 1.8).

A complementary series of X-ray photoelectron spectroscopy (XPS) experiments was conducted in order to ascertain the oxidation state(s) of the titanium oxide nanoparticles. Here, we focus on studies in which the initial titanium coverage was 0.27 ML which is expected to yield structures similar to those observed in the STM experiments for 0.25 ML of Ti (Fig. 3a).

Photoemission spectra collected from titanium-covered Au(111) surfaces before (a) as well as after oxidation (b) and subsequent annealing (c-d) are shown in Figure 4. The broad Ti(2p) feature observed after deposition of metallic titanium (Fig. 4a, left) suggests a slight oxygen contamination of the Ti filament used for Ti deposition. Indeed, oxygen is detected in the corresponding O(1s) spectrum (Fig. 4a, right) even after Ti is freshly evaporated. This oxygen was never completely eliminated, although the proportion of oxide deposited decreased as the experiments progressed in time (after the wire had been subjected to many evaporation cycles).

Considerable changes in both the Ti(2p) and the O(1s) region were observed after O_2 exposure (6.65×10^{-5} mbar / 200 s) at 300 K. The oxidation of titanium is clearly revealed by (i) a marked narrowing of the Ti(2p) signal (Fig. 4b, left) accompanied by a shift towards higher binding energy (BE) and (ii) an increase of the corresponding O(1s) signal (Fig. 4b, right). In comparison with single-crystal TiO_2, the full width at half maximum (FWHM) of the Ti($2p_{3/2}$) feature is still too large (1.75 eV versus 1.1 eV), and the BE is too low (458 eV versus 459.3 eV) (see also table I). These observations reveal that oxidation by O_2 exposure at room temperature does not produce a TiO_2 phase.

After oxidation at 300 K, oxygen seems to be associated with both titanium nanoparticles *and* the gold substrate as indicated by the breadth of the O(1s) line (FWHM of 2.6 eV versus 1.4 eV observed for TiO_2(110)). Specifically, curve-fitting of the O(1s) signal shown in Figure 4b suggests two components at 529.8 eV and 531.2 eV. Annealing experiments suggest (see below) that the 529.8 eV feature is linked to the formation of titanium oxide, whereas the 531.2 eV component seems to indicate the presence of excess oxygen adsorbed on the gold surface. However, this interpretation is not unambiguous as chemisorbed oxygen on Au(111) surfaces typically exhibits the O(1s) binding energies in the range of 529.8-530.1 eV [27].

The presence of excess oxygen adsorbed on the Au(111) surface is further corroborated by the fact that a quantitative analysis of the XPS data reveals a O:Ti ratio of 3.65 (rather than the expected O:Ti ratio of 2 for stoichiometric TiO_2). As O_2 does not chemisorb directly on Au(111) in the temperature range from 100 to 800 K [28, 29], the presence of excess oxygen indicates oxygen spillover from titanium nanoparticles to the gold surface. In order to prove the existence of adsorbed oxygen on the Au(111) surface, we performed separate temperature programmed desorption experiments. Indeed, O_2 evolution was observed to occur around 650 K (data not shown). For comparison, chemisorbed oxygen on Au(111) prepared by ozone exposure desorbs around 550 K [29], thus suggesting that the excess oxygen discussed above is not adsorbed on unperturbed gold, but is stabilized by the presence of the titanium oxide nanoparticles.

Annealing to 600 K in vacuum leads to the modification of the titanium oxide particles as revealed by a further increase of the Ti($2p_{3/2}$) binding energy from 458 to 458.5 eV (Fig. 4c, left). Note, that the Ti($2p_{3/2}$) binding energy is still considerably lower than that observed for of single-crystal TiO_2. Simultaneously, the O(1s) component at 529.8 eV narrows and shifts to 530.3 eV, accompanied by a small decrease in signal intensity (Fig. 4c, right). The marked decrease of the second O(1s) component at 531.2 eV seems to be related to the desorption of excess oxygen bound to the gold surface. It is possible that the O(1s) feature contains contributions from more than two peaks, because annealing results in the modification of the titanium oxide particles. However, no attempt was made to fit the peak with more than two features.

Stoichiometric TiO_2 nanoparticles are formed upon further annealing to 900 K in vacuum as illustrated by the Ti($2p_{3/2}$) signal at 459.3 eV (Figure 4d, left). This line position is identical to that obtained from single-crystal TiO_2 (Figure 4e, left). The corresponding O(1s) peak (Fig. 4d, right) also shifts to the BE value expected for stoichiometric TiO_2 (530.7 eV). A single oxidation state of titanium, Ti^{+4}, is further corroborated by observed XPS linewidths; the FWHM values of both Ti($2p_{3/2}$) (1.2 eV) and O(1s) features (1.5 eV) is almost identical to those observed in TiO_2(110), 1.1 eV and 1.4 eV, respectively. Furthermore, quantitative analysis of the XPS data indicates a O:Ti ratio of 2.12, consistent with the formation of stoichiometric TiO_2 nanoparticles. Note that the Ti coverage decreased from 0.27 ML to 0.19 ML after the 900 K anneal. This decrease may be due to diffusion of titanium metal into the Au. As noted above, Ti metal does dissolve into Au, rendering this explanation likely.

Summary

Titanium oxide nanoparticles supported on a reconstructed Au(111) surface were prepared by the deposition of titanium metal and subsequent oxidation. Initially, metal particles nucleate at the elbow sites of the herringbone reconstruction on the Au(111) surface. Subsequent oxidation and heating of these particles results in their aggregation towards nanocrystalline two- and three-dimensional titanium oxide particles. XPS line widths and binding energies reveal the presence of a single oxidation state of titanium corresponding to TiO_2.

Acknowledgements

The authors gratefully acknowledge the support of the National Science Foundation through NSF CTS 0000283. J.B. acknowledges current support under the auspices of the U. S. Department of Energy by the University of California, Lawrence Livermore National Laboratory, under Contract No. W-7405-Eng-48.

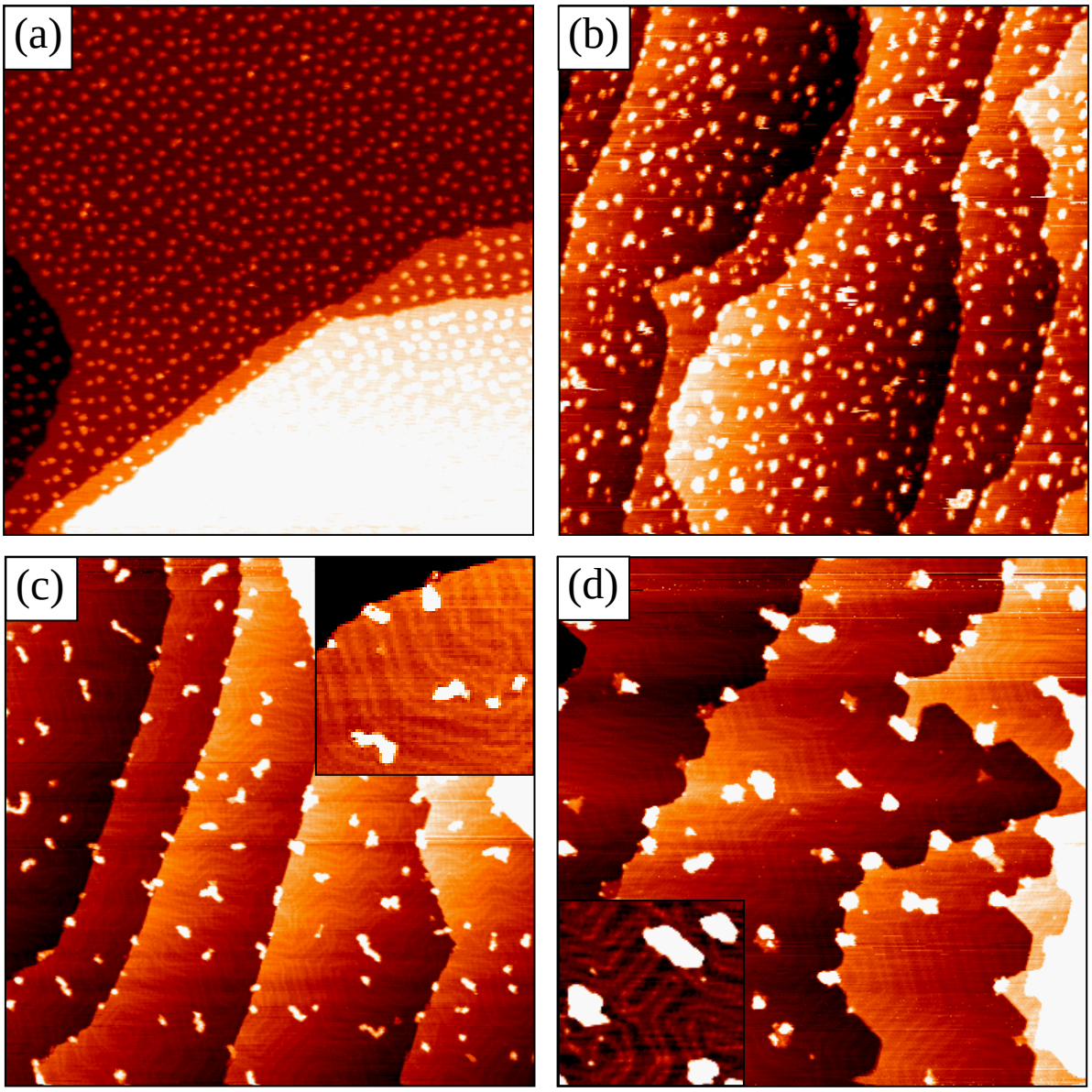

Figure 1

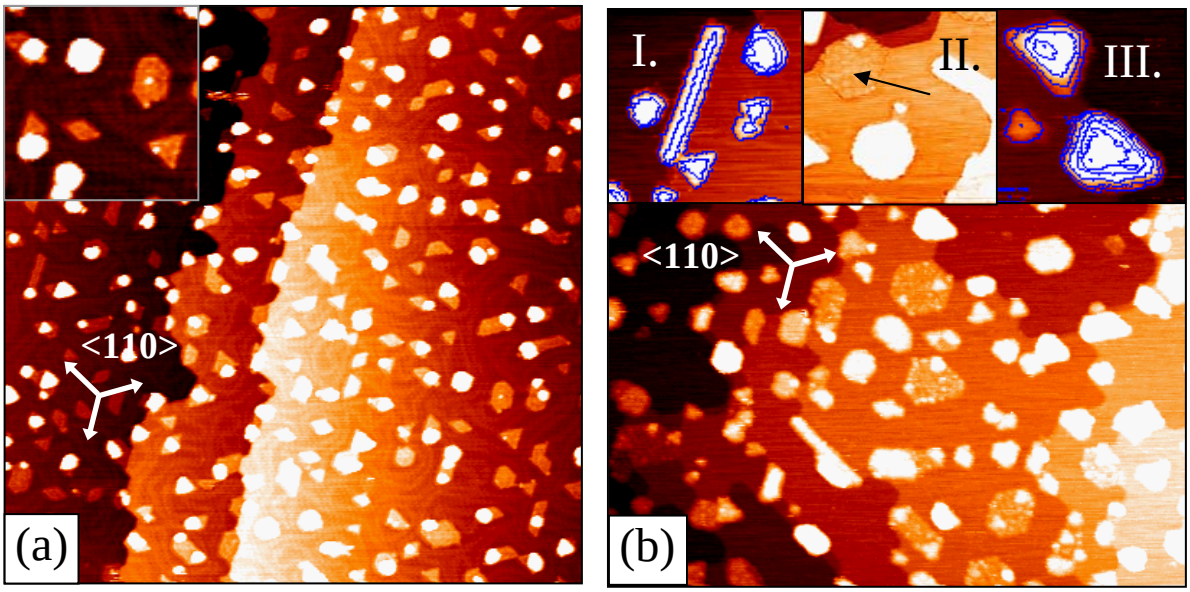

Figure 2

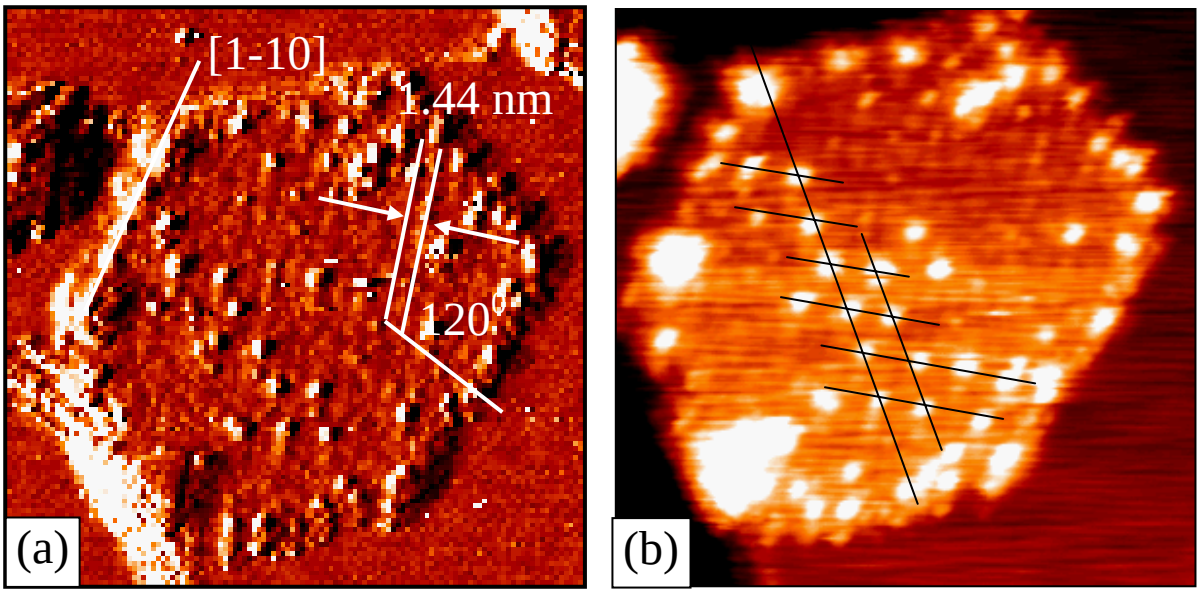

Figure 3

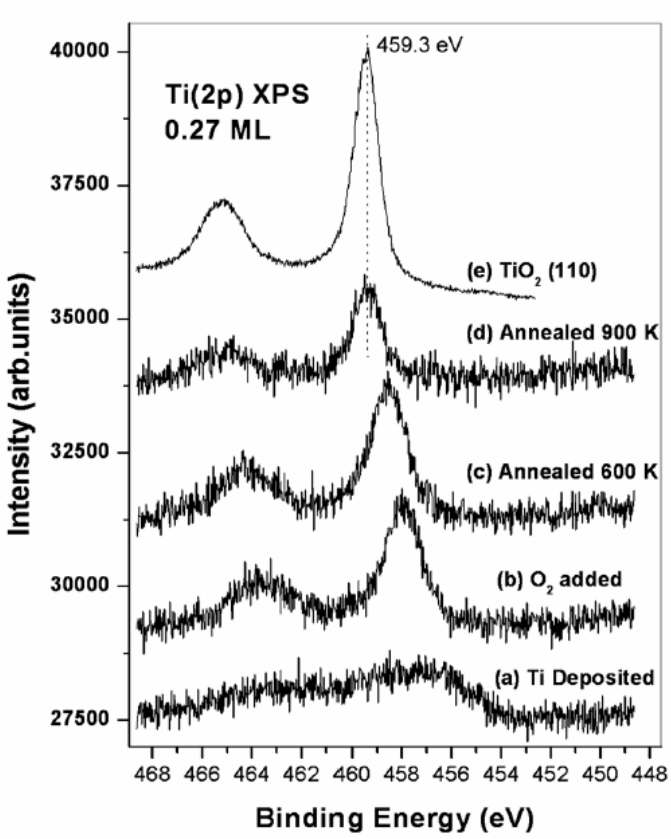
Ti(2p) XPS
0.27 ML
459.3 eV
(e) TiO2 (110)
(d) Annealed 900 K
(c) Annealed 600 K
(b) O2 added
(a) Ti Deposited
Intensity (arb.units)
Binding Energy (eV)
40000
37500
35000
32500
30000
27500
468 466 464 462 460 458 456 454 452 450 448

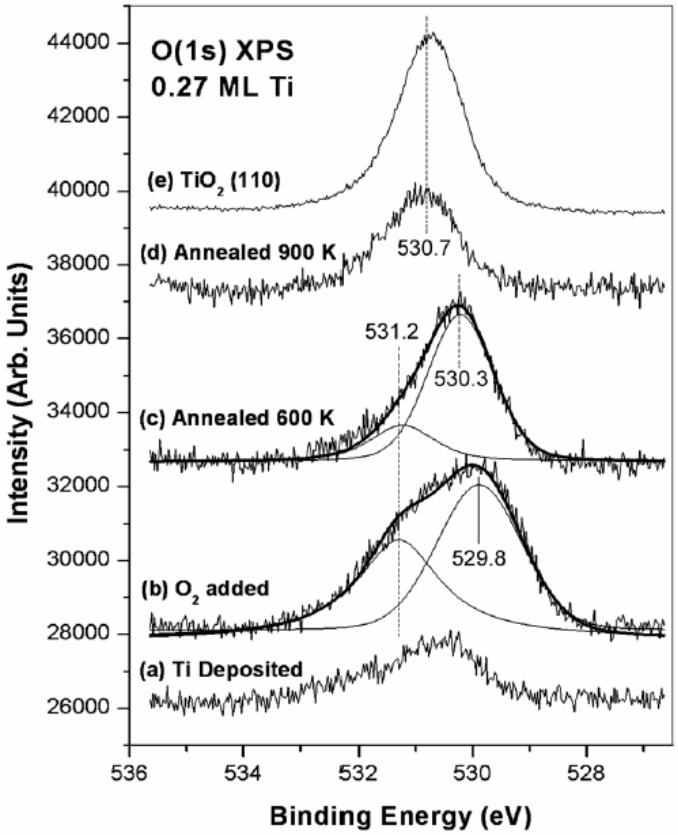
O(1s) XPS
0.27 ML Ti
(e) TiO2 (110)
(d) Annealed 900 K
530.7
531.2
530.3
(c) Annealed 600 K
529.8
(b) O2 added
(a) Ti Deposited
Intensity (Arb. Units)
Binding Energy (eV)
44000
42000
40000
38000
36000
34000
32000
30000
28000
26000
536 534 532 530 528

Figure 4

Table 1. XPS data for the vacuum anneal oxidation process of 0.27 ML titanium nanoparticles on a Au(111) surface (Data taken from Figure 4).

Description	**B. Energy Ti($2p_{3/2}$) (eV)**	**FWHM Ti($2p_{3/2}$) (eV)**	**B. Energy O(1s) (eV)**	**FWHM O(1s) (eV)**	**Ti θ (ML)**	**O θ (ML)**	**Ratio O/Ti**
Initially Deposited	(broad)	(broad)	530.6	1.7	0.27	0.37	1.37
10,000 L O_2 RT	458.0	1.8	530.1	2.6	0.27	0.99	3.65
Annealed 600 K	458.5	1.4	530.3	1.6	0.27	0.67	2.48
Annealed 900 K	459.3	1.2	530.7	1.5	0.19	0.40	2.12
TiO_2(110)	459.3	1.1	530.7	1.4	----	----	2.08

Figure Captions:

Figure 1: Series of STM images illustrating the morphological changes of Ti clusters on Au(111) due to oxidation and subsequent annealing. (a) Well-ordered arrays of Ti clusters are observed after PVD of 0.1 ML Ti at 300 K onto the reconstructed Au(111) surface. (b) Subsequent oxidation of the Ti clusters by O_2 exposure (5×10^{-5} mbar × 200 s) at 300 K leads to disordering and growth of the particles. Faceted 3D titanium oxide crystallites are observed after annealing to 600 K (c), and 900 K (d), respectively (10 minutes at each temperature). Note the serrated, <110> oriented Au step edge morphology after annealing to 900 K. Details of the herringbone reconstruction and the "turns" around the oxide particles are shown in the insets. The images correspond to an area of 200 nm × 200 nm (a, b, c) and 160 nm × 160 nm (d). The insets correspond to an area of 40 nm x 40 nm.

Figure 2: STM images of 2D and 3D titanium oxide nanocrystallites prepared by oxidation (O_2, 5×10^{-5} mbar × 200 s) of 0.25 ML Ti (a) and 0.5 ML Ti (b), respectively, followed by annealing at 900 K (10 minutes). The crystallites are aligned with the substrate and have triangular or hexagonal shape. (b) Additional features such as needle-like crystallites (inset I) and embedded hexagons (inset II) are observed for the higher Ti starting coverage (b). Contour lines, equally spaced by 0.5 nm, are used to visualize the crystallinity of the 3D Ti oxide particles.
The images correspond to an area of (a): 160 × 160 nm, inset: 32 nm × 32 nm and (b): 200 nm × 200 nm, insets: 50 nm × 50 nm (I), 52 nm × 52 nm (II), 30 × 30 nm (III).

Figure 3: Detail of the preparation shown in figure 2b illustrating the crystallinity of a 2D titanium oxide island. (a) The I-channel image reveals two sets of rows which are separated by ~1.4 nm and rotated by ~120° against each other. The rows are rotated ~10° against the close-packed <110> directions of the substrate. (b) The Z-channel image shows additional second layer features on top of the titanium oxide island which seem to exhibit a $(\sqrt{3} \times \sqrt{3})R30°$ relationship towards the underlying structure. The images correspond to an area of 47 nm × 47 nm (a), and 41 nm × 41 nm (b).

Figure 4: Ti(2p) (left panel) and O(1s) (right panel) X-ray photoelectron spectra collected from titanium-covered Au(111) surfaces before (a) as well as after oxidation (6.65×10^{-5} mbar O_2 / 200 s) at 300 K (b) and subsequent annealing at 600 K (c) and 900 K (d), respectively. The initial Ti coverage is 0.27 ML. Reference data collected from a clean TiO_2(110) single crystal are shown in (e). All spectra were collected at 300 K.

References

1 U. Diebold, Surface Science Reports 48 (2003) 53.
2 Q. Wang and R. J. Madix, Surface Science 496 (2002) 51.
3 G. Deo and I. E. Wachs, Journal of Catalysis 146 (1994) 323.
4 I. E. Wachs, G. Deo, M. V. Juskelis, and B. M. Weckhuysen, Stud. Surf. Sci. Catal. 109 (1997) 305.
5 P. Forzatti, E. Tronconi, A. Elmi, and G. Busca, Appl. Cat. A 157 (1997) 387.
6 M. Valden, S. Pak, X. Lai, and D. W. Goodman, Catal. Lett. 56 (1998) 7.
7 X. Lai, T. P. St Clair, M. Valden, and D. W. Goodman, Prog. Surf. Sci. 59 (1998) 25.
8 D. A. H. Cunningham, W. Vogel, H. Kageyama, S. Tsubota, and M. Haruta, J. Cat. 177 (1998) 1.
9 F. H. Iizuka Y, Yamauchi N, Chijiiwa T, Arai S, Tsubota S, Haruta M, Catalysis Today 36 (1997) 115.
10 H. M. Sakurai H, Catalysis Today 29 (1996) 361.
11 M. Valden, X. Lai, and D. W. Goodman, Science 281 (1998) 1647.
12 M. M. Biener, J. Biener, and C. M. Friend, submitted
13 J. A. Rodriguez, M. Perez, T. Jirsak , J. Evans, J. Hrbek, and L. Gonzalez, Chem. Phys. Lett. 378 (2003) 526.
14 G. Mills, M. S. Gordon, and H. Metiu, J. Chem. Phys. 118 (2003) 4198.
15 M. M. Biener and C. M. Friend, Surf. Sci. Lett. 559 (2004) L173.
16 M. M. Biener, J. Biener, R. Schalek, and C. M. Friend, J. Chem. Phys. (in press)
17 S. Y. Quek, M. M. Biener, J. Biener, C. M. Friend, and E. Kaxiras, (to be published)
18 M. M. Biener, J. Biener, R. Schalek, and C. M. Friend, Surf. Sci. (submitted)
19 D. Chambliss, R. Wilson, and S. Chiang, Phys. Rev. Let. 66 (1991) 1721.
20 J. A. Stroscio, D. T. Pierce, R. A. Dragoset, and P. N. First, J. Vac. Sci. Technol. A 10 (1992) 1981.
21 B. Voigtlaender, G. Meyer, and N. Amer, Phys. Rev. B 44 (1991) 10354.
22 S. Helveg, J. V. Lauritsen, E. Laegsgaard, I. Stensgaard, J. K. Norskov, B. S. Clausen, H. Topsoe, and F. Besenbacher, Phys. Rev. Lett. 84 (2000) 951.
23 Z. Song, T. Cai, J. A. Rodriguez, J. Hrbek, A. S. Y. Chan, and C. M. Friend, J. Phys. Chem. B 107 (2003) 1036.
24 Q. Wang, Ph.D. Thesis, Stanford University (2001)
25 J. Biener, (to be published)
26 A. Berko, G. Menesi, and F. Solymosi, Surf. Sci 372 (1996) 202.
27 M. A. Lazaga, D. T. Wickham, D. H. Parker, G. N. Kastanas, and B. E. Koel, in *Catalytic Selective Oxidation*, edited by S. T. Oyama and J. W. Hightower (American Chemical Society, Washington D.C., 1993), Vol. 523, p. 90.
28 J. J. Pireaux, M. Chtaib, J. P. Delrue, P. A. Thiry, M. Liehr, and R. Caudano, Surface Science 141 (1984) 211.
29 D. H. Parker and B. E. Koel, Journal of Vacuum Science and Technology A 8 (1990) 2585.